Mon. Not. R. astr. Soc. (1990) **247**, 632–646

Spots on AG Virginis – paradigm or panacea?★

S. A. Bell, P. P. Rainger and R. W. Hilditch
University Observatory, Buchanan Gardens, St. Andrews, Fife KY16 9LZ

Accepted 1990 July 5. Received 1990 July 3; in original form 1990 May 24

SUMMARY

New photometric and spectroscopic observations of the eclipsing binary AG Vir are presented. Medium-resolution spectroscopy has allowed the measurement of velocities for the secondary component for the first time. The *V* light curve shows many of the features seen in previous studies of this system. A full analysis of the spectroscopic and photometric data has been made which suggests that the system is either in a marginal state of contact or a deep-contact configuration depending on the type of spot model invoked. AG Vir constitutes an excellent example of the expected manifestations of spot activity on a light curve. It also demonstrates the ease with which the spot phenomenon can be invoked to explain the appearance of a light curve and to provide conflicting results. This study shows the necessity of a more thorough investigation of this system using Doppler-imaging techniques and simultaneous infrared and optical photometry.

1 INTRODUCTION

The eclipsing binary AG Vir (HD 104350, BD + 13° 2481) has been the subject of several studies during the past 60 years since its discovery by Guthnick & Prager (1929). The period of the system was correctly determined by Dugan (1933) and two photographic studies were subsequently made by Bodokia (1937) and Gaposchkin (1953). Several photoelectric light curves have been presented for this W Ursae–Majoris system by Wood (1946), Szczepanowska (1958), Fliegel (1963), Binnendijk (1969), Blanco & Catalano (1970) and more recently by Niarchos (1985) and Kałużny (1986). Low-dispersion spectroscopic observations (≈ 79 Å mm^{-1}) have been made by Sanford (1934) who measured radial velocities for the brighter component only, and by Hill & Barnes (1972) who obtained similar observations (≈ 63 Å mm^{-1}) and also found no evidence for the spectrum of the secondary component. They concluded that the orbit of AG Vir was eccentric and presented orbital elements for the system.

In the majority of published light curves, the bottom of primary minimum is somewhat distorted and shows some evidence for night-to-night variations (e.g. Michaels 1988). Similarly, first quadrature is also considerably brighter than second quadrature by approximately 0.08 mag and secondary minimum occurs shortly after 0^p.5. Binnendijk (1969) has shown that the orbital period of AG Vir abruptly lengthened by 0.4 s around 1944. Blanco & Catalano (1970) subsequently suggested that the orbital period of the system shows a variation in an interval of just under 40 yr. However, times of minima obtained since their study suggest that this interpretation is probably no longer applicable. The period of this system appears to have been constant since 1944 although the residuals of the photoelectric times of minima from a specific ephemeris show a scatter of around 0.005 d, more than would normally be expected for photoelectric data. These variations and the distortions in the light curves have been put forward as evidence for gas streams and/or spot activity on one or both of the components of AG Vir (e.g. Kałużny 1986). A study of chromospheric emission from 14 W UMa systems by Eaton (1983) using short-wavelength *IUE* spectra indicated that AG Vir showed little clear evidence of surface activity, whereas A-type systems of similar spectral type such as V535 Ara and S Ant showed considerable activity.

In view of the nature of the light curve of AG Vir and the possibility of spot activity being responsible for the difference in the luminosity of the two quadratures and also the phase delay of secondary minimum, it was decided to include this system in a study of contact binaries at St. Andrews. Kałużny (1986) has pointed out the need for higher dispersion spectroscopy to recover the secondary component spectrum in order to obtain accurate radial-velocity curves for both components and to determine a mass ratio which is independent of light-curve analyses. Consequently, a full photometric and spectroscopic analysis has been made to determine the physical properties of the system and to study the role of localized spot activity on the appearance of the light curve. In this study, photoelectric photometry made during 1989 and radial-velocity data for both components obtained during 1988 are presented.

★ Based in part upon observations obtained at the Observatorio del Roque de los Muchachos, Canary Islands, Spain.

2 SPECTROSCOPY

2.1 Observations

The spectroscopic observations of AG Vir were obtained by PPR during the period 1988 April 28–May 2 at the Observatorio del Roque de los Muchachos, La Palma, with the 2.5-m Isaac Newton Telescope (INT), the Intermediate Dispersion Spectrograph (IDS) and GEC CCD detector. The Jobin–Yvon 1200 grating was employed in conjunction with the 500-mm camera of the IDS to provide spectra at a dispersion of 16.7 Å mm^{-1}. Each spectrum was centred on 4200 Å with a useful range of approximately 200 Å. The integration times for the programme-star spectra were typically 800 s (<2 per cent of the orbital period) allowing data to be obtained at a signal-to-noise ratio of approximately 25–30 while maintaining adequate time resolution.

Observations of radial-velocity standard stars with spectral types of between F0 and F6 were also made at regular intervals during each night to calibrate the system. Subsequently, some of these observations were used as comparison-star spectra in cross-correlation analyses of the AG Vir data. All stellar integrations were alternated with comparison-source exposures using an Cu–Ar lamp for wavelength calibration purposes.

2.2 Reduction and analysis

Preliminary reductions of the spectroscopic data were made via the STARLINK software package FIGARO which included the removal of cosmic-ray events, bias subtraction, flat-fielding and sky background subtraction. The resulting data were converted into a one-dimensional form for processing with the spectroscopic image-processing package REDUCE (Hill, Fisher & Poeckert 1982). The spectra were linearized, rectified and finally log-linearized using REDUCE in preparation for the cross-correlation analysis using VCROSS (Hill 1982). The cross-correlation functions were optimized by defining windows across the useful range of the spectra omitting the broad asymmetric Ca I feature at λ4226 Å.

The spectra of the radial-velocity standard stars observed during the run were cross-correlated against each other and measured by fitting a single Gaussian profile to the resulting cross-correlation functions. The mean residual in the sense of standard minus observed was -1.7 ± 7.0 (s.d.) km s^{-1} indicating that the observations were compatible with the standard system. No dependence on either hour angle or zenith distance was found.

The spectra of AG Vir were cross-correlated against the F6IV standard star HD 89449 as this combination produced the most clearly defined peaks in the cross-correlation functions. Gaussian profiles were fitted to the cross-correlation functions by least squares and where necessary, double Gaussian profiles were employed for the double-line phases. The resulting radial-velocity measurements and their times of observation are given in Table 1. These observations were phased using the ephemeris computed in Section 4. Four of the 19 spectra yielded unacceptably broad cross-correlation functions and were not included in the analysis although they appear in Table 1 for the sake of completeness only. The cross-correlation functions are presented in Fig. 1.

A careful analysis of the limited number of radial-velocity data for each component gives no indication of any orbital eccentricity e. If spot activity is present in the light curve near 0ᵖ.5, it would be unwise to draw any conclusive evidence for orbital eccentricity from the phase delay of secondary minimum. Therefore, circular orbits have been adopted for this analysis. The radial-velocity data set for each component was fitted with a sine wave by means of a least-squares analysis within PULSAR (Skillen 1985). The radial-velocity semi-amplitudes for the primary and secondary components, K_1 and K_2, respectively, the systemic velocity V_0 and the derived mass functions and projected semi-major axes of the orbits and their standard errors are given in Table 2. The radial-velocity data, the computed orbits and their respective residuals are plotted in Fig. 2.

It would appear that the orbital eccentricity calculated by Hill & Barnes (1972) can be explained in terms of the blending of lines from both components of AG Vir caused by the measurement of low-dispersion spectroscopy. The small number of spectra obtained for this study make an accurate determination of the systemic velocity difficult and probably contribute to the difference between the values determined from the primary and secondary component velocity curves. However, there is reasonable agreement between the values of K_1 and $\bar{V}_0$ determined in this study and that of Hill & Barnes. The relatively limited wavelength range observed for this study precluded any attempt to make a spectral classification for AG Vir.

Table 1. Radial-velocity data for AG Vir.

H.J.D.	Phase	V_1	(O–C)	V_2	(O–C)
		km s^{-1}	km s^{-1}	km s^{-1}	km s^{-1}
2447280.46673	0.6737	+65	−1.4	−207	−7.2
2447281.45247	0.2075	−74	−0.2	+238	−8.2
2447282.38671	0.6612	+61	−2.5	−195	−4.6
2447282.41375	0.7033	+72	+0.3	−211	+5.6
2447282.42605	0.7225	+74	+0.2	−220	+3.3
2447282.45757	0.7715	+77	+2.7	−221	+3.7
2447282.51917	0.8674	+53	−2.3	−170	−5.7
2447282.53419	0.8907	+51	+3.8	−135	+3.8
2447282.59610	0.9871	——	——	——	——
2447282.62605	0.0337	——	——	——	——
2447283.39107	0.2241	−78	−2.5	+248	−3.6
2447283.40571	0.2469	−74	+2.5	+251	−3.7
2447283.42045	0.2698	−75	+0.9	+255	+2.1
2447283.44870	0.3138	−72	−1.5	+248	+12.3
2447283.46098	0.3329	−66	+0.4	+225	+2.2
2447283.50243	0.3974	——	——	——	——
2447283.53190	0.4432	−26	+1.2	——	——
2447283.56198	0.4900	——	——	——	——
2447283.59209	0.5369	+15	−1.6	——	——

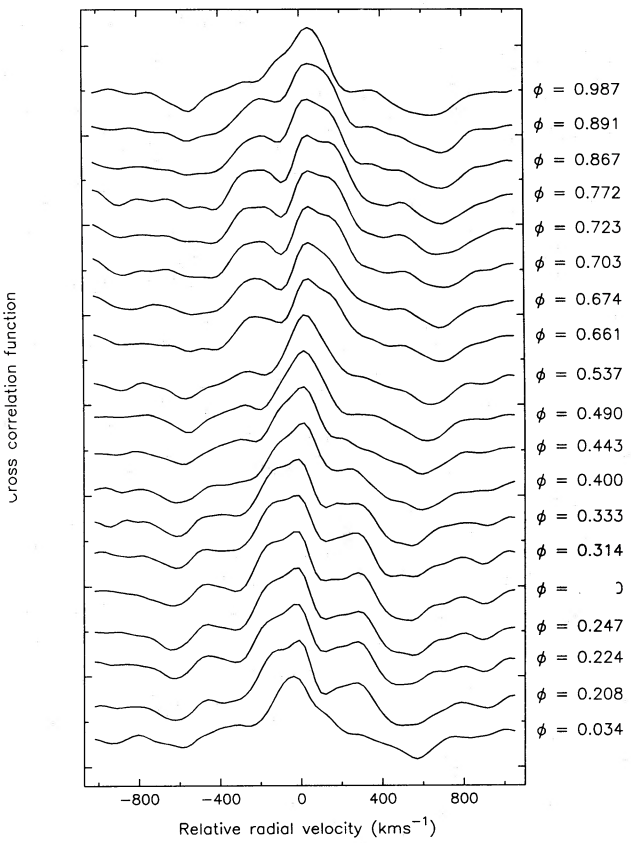

Figure 1. The cross-correlation functions for the 19 spectra obtained for this study. The orbital phase for each cross-correlation function is also given.

3 PHOTOMETRIC OBSERVATIONS AND REDUCTIONS

Photoelectric photometry was obtained by SAB and PPR with the Twin Photometric Telescope (TPT) at St. Andrews on 1989 March 7/8, 10/11 and 15/16. The observing technique has been described in more detail elsewhere (Bell & Hilditch 1984). The filter employed for these observations is comparable to the Johnson V filter. The integration times were fixed at 60 s and a 40 arcsec diaphragm was employed throughout the observing run. The data were reduced with the computer program SIMPHOT written by one of us (SAB) which follows the method described by Hilditch (1981).

The comparison and check stars used for this study were BD + 13° 2485 and BD + 13° 2482, respectively. The comparison star has been used extensively in the majority of studies of AG Vir; however, for convenience of observing with the TPT, BD + 13° 2482 was chosen as the check star in place of BD + 13° 2405 which has been employed in previous studies. No evidence for variability in the comparison star has been found in previous investigations and the differential magnitudes in the sense check minus comparison calculated for this study were stable to better than 0.01 mag. The typical error in the differential magnitudes for the light curves of AG Vir is approximately 0.006 mag. The photoelectric data consisting of 663 observations are listed in Table 3 and plotted in Fig. 3. The data in Table 3 are in the instrumental system as the colour term in the transformation to the standard system is negligible for the TPT/photometer combinations.

Table 2. Orbital elements for AG Vir.

K_1 (km s^{-1})	=	75.7 ± 0.6
K_2 (km s^{-1})	=	240.8 ± 1.9
V_{0_1} (km s^{-1})	=	−0.8 ± 0.5
V_{0_2} (km s^{-1})	=	+13.9 ± 1.7
$\overline{V}_0$ (km s^{-1})	=	−6.6 ± 1.8
σ_1 (km s^{-1}) †	=	2.0
σ_2 (km s^{-1}) †	=	6.0
q (m_2/m_1)	=	0.314 ± 0.004
e	=	0 (adopted)
$a_1 \cdot \sin i$ ($R_\odot$)	=	0.961 ± 0.008
$a_2 \cdot \sin i$ ($R_\odot$)	=	3.058 ± 0.024
$a \cdot \sin i$ ($R_\odot$)	=	4.019 ± 0.025
$m_1 \cdot \sin^3 i$ ($M_\odot$)	=	1.611 ± 0.024
$m_2 \cdot \sin^3 i$ ($M_\odot$)	=	0.506 ± 0.008

† Rms error in an observation.

Examination of the light curve reveals several interesting features. The most noticeable is the fact that first quadrature is 0.09 mag brighter than second quadrature. There is a well-defined anomalous brightening of the system during the egress from primary minimum between 0^p.00 and 0^p.04. On closer examination, the phase of maximum light near first quadrature is displaced by 0^p.02 towards primary minimum, whereas maximum light at second quadrature occurs at 0^p.75. The middle of the 'flat' portion of secondary minimum occurs at 0^p.515 although extrapolation of the ingress to and egress from this minimum suggests that secondary minimum occurs at 0^p.5. Finally, the 'flat' portion of secondary minimum is not quite flat – there appears to be a very slow increase in brightness through the bottom of the eclipse.

4 EPHEMERIS

Binnendijk (1969) showed that the period of AG Vir increased abruptly by 0.4 s around 1944 and noted that secondary minimum generally occurs later than 0^p.5. He deduced that the period had been constant since 1944 and computed the following ephemeris:

primary minimum (HJD) = 2439946.7472 + 0.64265068.E.

Blanco & Catalano (1970) concluded that the orbital period suffers a slow variation with a period of just less than 40 yr. Subsequently, it was suggested by Niarchos (1985) that if this variation was real then a third body or apsidal motion could be invoked to explain the variation. Michaels (1988) has demonstrated that the displacement of secondary minimum shows evidence of increasing slowly with time over the past 50 yr, and that the period change around 1944 was 0.11 s deduced from times of photoelectric primary minima only. His analysis has also cast doubt on the 40-yr variation suggested by Blanco & Catalano. Kałużny (1986) has sug

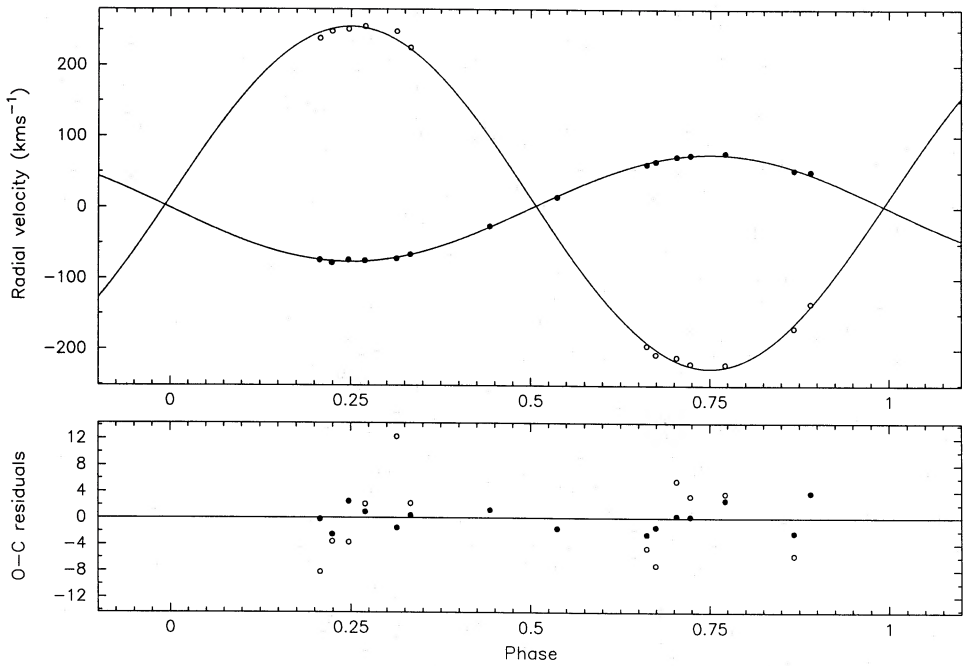

Figure 2. Observed radial velocities and computed orbits for AG Vir. Filled circles represent primary component data and open circles represent secondary component data. The lower plot shows the residuals of the observations of both components from their respective computed orbits.

Table 3. TPT V observations.

H.J.D.	Phase	(V–C)	H.J.D.	Phase	(V–C)	H.J.D.	Phase	(V–C)
2447593.41060	0.6317	+1.598	2447593.47414	0.7306	+1.467	2447593.54136	0.8352	+1.540
2447593.41129	0.6328	+1.602	2447593.47483	0.7316	+1.462	2447593.54205	0.8362	+1.536
2447593.41198	0.6338	+1.591	2447593.47553	0.7327	+1.474	2447593.54275	0.8373	+1.544
2447593.41268	0.6349	+1.588	2447593.47622	0.7338	+1.477	2447593.54417	0.8395	+1.550
2447593.41337	0.6360	+1.588	2447593.47797	0.7365	+1.478	2447593.54487	0.8406	+1.552
2447593.41503	0.6386	+1.563	2447593.47867	0.7376	+1.471	2447593.54556	0.8417	+1.559
2447593.41572	0.6397	+1.574	2447593.47936	0.7387	+1.466	2447593.54626	0.8428	+1.560
2447593.41642	0.6408	+1.570	2447593.48005	0.7398	+1.470	2447593.54695	0.8439	+1.556
2447593.41711	0.6418	+1.576	2447593.48075	0.7409	+1.473	2447593.55578	0.8576	+1.572
2447593.41782	0.6429	+1.566	2447593.48748	0.7513	+1.466	2447593.55649	0.8587	+1.571
2447593.42160	0.6488	+1.561	2447593.48818	0.7524	+1.461	2447593.55717	0.8598	+1.574
2447593.42230	0.6499	+1.552	2447593.48887	0.7535	+1.466	2447593.55786	0.8608	+1.589
2447593.42299	0.6510	+1.561	2447593.48957	0.7546	+1.473	2447593.55856	0.8619	+1.585
2447593.42369	0.6521	+1.553	2447593.49026	0.7557	+1.468	2447593.56128	0.8662	+1.591
2447593.42438	0.6531	+1.557	2447593.49161	0.7578	+1.473	2447593.56197	0.8672	+1.600
2447593.42600	0.6557	+1.537	2447593.49231	0.7588	+1.473	2447593.56267	0.8683	+1.601
2447593.42670	0.6567	+1.546	2447593.49300	0.7599	+1.468	2447593.56336	0.8694	+1.614
2447593.42739	0.6578	+1.544	2447593.49370	0.7610	+1.467	2447593.56406	0.8705	+1.601
2447593.42808	0.6589	+1.553	2447593.49439	0.7621	+1.478	2447593.56518	0.8722	+1.602
2447593.42878	0.6600	+1.539	2447593.49524	0.7634	+1.474	2447593.56587	0.8733	+1.614
2447593.43039	0.6625	+1.541	2447593.49593	0.7645	+1.484	2447593.56657	0.8744	+1.612
2447593.43108	0.6636	+1.538	2447593.49663	0.7656	+1.473	2447593.56726	0.8755	+1.611
2447593.43178	0.6647	+1.538	2447593.49732	0.7666	+1.482	2447593.56797	0.8766	+1.607
2447593.43247	0.6657	+1.535	2447593.49801	0.7677	+1.474	2447593.57282	0.8841	+1.625
2447593.43317	0.6668	+1.531	2447593.50054	0.7716	+1.471	2447593.57351	0.8852	+1.628
2447593.43462	0.6691	+1.518	2447593.50123	0.7727	+1.475	2447593.57421	0.8863	+1.625
2447593.43532	0.6702	+1.526	2447593.50193	0.7738	+1.477	2447593.57490	0.8874	+1.639
2447593.43601	0.6712	+1.530	2447593.50262	0.7749	+1.475	2447593.57560	0.8884	+1.637
2447593.43671	0.6723	+1.529	2447593.50332	0.7760	+1.476	2447593.57792	0.8921	+1.649
2447593.43740	0.6734	+1.528	2447593.50542	0.7792	+1.478	2447593.57862	0.8931	+1.647
2447593.43926	0.6763	+1.520	2447593.50612	0.7803	+1.482	2447593.57931	0.8942	+1.656
2447593.43995	0.6774	+1.516	2447593.50681	0.7814	+1.470	2447593.58001	0.8953	+1.661
2447593.44064	0.6784	+1.510	2447593.50751	0.7825	+1.479	2447593.58070	0.8964	+1.661
2447593.44134	0.6795	+1.515	2447593.50820	0.7836	+1.484	2447593.58317	0.9002	+1.670
2447593.44203	0.6806	+1.508	2447593.51271	0.7906	+1.485	2447593.58386	0.9013	+1.677

Table 3 – *continued.*

H.J.D.	Phase	(V–C)	H.J.D.	Phase	(V–C)	H.J.D.	Phase	(V–C)
2447593.44644	0.6875	+1.507	2447593.51341	0.7917	+1.478	2447593.58455	0.9024	+1.677
2447593.44714	0.6886	+1.506	2447593.51410	0.7927	+1.485	2447593.58525	0.9035	+1.679
2447593.44783	0.6896	+1.512	2447593.51480	0.7938	+1.481	2447593.58594	0.9045	+1.686
2447593.44852	0.6907	+1.510	2447593.51549	0.7949	+1.485	2447593.58800	0.9077	+1.691
2447593.44922	0.6918	+1.504	2447593.51704	0.7973	+1.500	2447593.58870	0.9088	+1.699
2447593.45049	0.6938	+1.496	2447593.51774	0.7984	+1.482	2447593.58939	0.9099	+1.691
2447593.45119	0.6949	+1.487	2447593.51843	0.7995	+1.484	2447593.59010	0.9110	+1.696
2447593.45187	0.6959	+1.499	2447593.51913	0.8006	+1.492	2447593.59078	0.9121	+1.706
2447593.45256	0.6970	+1.490	2447593.51982	0.8016	+1.491	2447593.59276	0.9151	+1.716
2447593.45326	0.6981	+1.503	2447593.52829	0.8148	+1.508	2447593.59345	0.9162	+1.715
2447593.46247	0.7124	+1.481	2447593.52899	0.8159	+1.512	2447593.59415	0.9173	+1.731
2447593.46317	0.7135	+1.482	2447593.52968	0.8170	+1.512	2447593.59484	0.9184	+1.724
2447593.46386	0.7146	+1.484	2447593.53038	0.8181	+1.512	2447593.59554	0.9195	+1.735
2447593.46455	0.7156	+1.487	2447593.53108	0.8192	+1.512	2447593.59735	0.9223	+1.735
2447593.46525	0.7167	+1.482	2447593.53275	0.8218	+1.519	2447593.59805	0.9234	+1.743
2447593.46648	0.7186	+1.486	2447593.53344	0.8228	+1.525	2447593.59874	0.9245	+1.753
2447593.46716	0.7197	+1.480	2447593.53414	0.8239	+1.518	2447593.59944	0.9255	+1.752
2447593.46785	0.7208	+1.479	2447593.53483	0.8250	+1.520	2447593.60013	0.9266	+1.762
2447593.46855	0.7219	+1.476	2447593.53553	0.8261	+1.515	2447593.60433	0.9332	+1.796
2447593.46924	0.7229	+1.476	2447593.53997	0.8330	+1.533	2447593.60503	0.9342	+1.794
2447593.47344	0.7295	+1.475	2447593.54067	0.8341	+1.540	2447593.60572	0.9353	+1.801
2447593.60642	0.9364	+1.798	2447593.67876	0.0490	+1.883	2447596.53791	0.4980	+1.875
2447593.60711	0.9375	+1.797	2447593.67945	0.0500	+1.870	2447596.53861	0.4991	+1.876
2447593.60902	0.9404	+1.803	2447593.68014	0.0511	+1.868	2447596.54010	0.5014	+1.873
2447593.60972	0.9415	+1.827	2447593.68152	0.0533	+1.863	2447596.54079	0.5025	+1.870
2447593.61041	0.9426	+1.829	2447593.68222	0.0544	+1.855	2447596.54149	0.5035	+1.871
2447593.61110	0.9437	+1.847	2447593.68291	0.0554	+1.847	2447596.54218	0.5046	+1.874
2447593.61180	0.9448	+1.841	2447593.68360	0.0565	+1.837	2447596.54288	0.5057	+1.872
2447593.61333	0.9472	+1.853	2447593.68430	0.0576	+1.849	2447596.54434	0.5080	+1.865
2447593.61402	0.9482	+1.862	2447593.68570	0.0598	+1.815	2447596.54503	0.5091	+1.875
2447593.61472	0.9493	+1.863	2447593.68639	0.0608	+1.820	2447596.54572	0.5101	+1.869
2447593.61541	0.9504	+1.873	2447593.68709	0.0619	+1.818	2447596.54642	0.5112	+1.870
2447593.61610	0.9515	+1.883	2447593.68778	0.0630	+1.809	2447596.54711	0.5123	+1.876
2447593.62028	0.9580	+1.903	2447593.68848	0.0641	+1.799	2447596.54893	0.5151	+1.869
2447593.62098	0.9591	+1.920	2447593.69210	0.0697	+1.774	2447596.54963	0.5162	+1.869
2447593.62167	0.9601	+1.914	2447593.69279	0.0708	+1.753	2447596.55033	0.5173	+1.870
2447593.62237	0.9612	+1.926	2447593.69349	0.0719	+1.767	2447596.55101	0.5184	+1.873
2447593.62307	0.9623	+1.932	2447593.69420	0.0730	+1.765	2447596.55171	0.5194	+1.868
2447593.62491	0.9652	+1.945	2447593.69488	0.0741	+1.751	2447596.55312	0.5216	+1.876
2447593.62561	0.9663	+1.956	2447593.69626	0.0762	+1.724	2447596.55382	0.5227	+1.868
2447593.62630	0.9673	+1.952	2447593.69695	0.0773	+1.726	2447596.55451	0.5238	+1.868
2447593.62700	0.9684	+1.959	2447593.69764	0.0783	+1.725	2447596.55520	0.5249	+1.864
2447593.62770	0.9695	+1.963	2447593.69834	0.0794	+1.722	2447596.55590	0.5260	+1.870
2447593.64363	0.9943	+2.006	2447593.69903	0.0805	+1.715	2447596.55738	0.5283	+1.870
2447593.64431	0.9954	+2.004	2447593.70034	0.0825	+1.709	2447596.55806	0.5293	+1.867
2447593.64501	0.9965	+2.003	2447593.70104	0.0836	+1.724	2447596.55876	0.5304	+1.867
2447593.64570	0.9975	+2.005	2447593.70173	0.0847	+1.705	2447596.55945	0.5315	+1.869
2447593.64639	0.9986	+2.005	2447593.70244	0.0858	+1.693	2447596.56015	0.5326	+1.867
2447593.64759	0.0005	+1.991	2447593.70312	0.0869	+1.702	2447596.56348	0.5378	+1.865
2447593.64827	0.0015	+1.996	2447596.51594	0.4638	+1.823	2447596.56417	0.5388	+1.864
2447593.65174	0.0069	+1.999	2447596.51664	0.4649	+1.831	2447596.56487	0.5399	+1.862
2447593.65244	0.0080	+1.995	2447596.51733	0.4659	+1.829	2447596.56556	0.5410	+1.857
2447593.65313	0.0091	+1.981	2447596.51803	0.4670	+1.835	2447596.56626	0.5421	+1.857
2447593.65382	0.0102	+1.987	2447596.51872	0.4681	+1.846	2447596.56753	0.5441	+1.845
2447593.65452	0.0113	+1.980	2447596.51975	0.4697	+1.843	2447596.56822	0.5451	+1.857
2447593.65695	0.0150	+1.971	2447596.52045	0.4708	+1.856	2447596.56892	0.5462	+1.845
2447593.65764	0.0161	+1.964	2447596.52114	0.4719	+1.847	2447596.56961	0.5473	+1.849
2447593.65834	0.0172	+1.953	2447596.52184	0.4730	+1.857	2447596.57031	0.5484	+1.843
2447593.65903	0.0183	+1.958	2447596.52253	0.4740	+1.857	2447596.57166	0.5505	+1.830
2447593.65973	0.0194	+1.958	2447596.52370	0.4759	+1.861	2447596.57236	0.5516	+1.828
2447593.66121	0.0217	+1.960	2447596.52439	0.4769	+1.871	2447596.57305	0.5527	+1.832
2447593.66190	0.0227	+1.954	2447596.52510	0.4780	+1.865	2447596.57375	0.5537	+1.827

Table 3 – *continued.*

H.J.D.	Phase	(V–C)	H.J.D.	Phase	(V–C)	H.J.D.	Phase	(V–C)
2447593.66260	0.0238	+1.960	2447596.52578	0.4791	+1.871	2447596.57444	0.5548	+1.818
2447593.66329	0.0249	+1.944	2447596.52648	0.4802	+1.874	2447596.57594	0.5571	+1.806
2447593.66400	0.0260	+1.950	2447596.52765	0.4820	+1.874	2447596.57664	0.5582	+1.816
2447593.66800	0.0322	+1.938	2447596.52834	0.4831	+1.873	2447596.57733	0.5593	+1.804
2447593.66869	0.0333	+1.942	2447596.52904	0.4842	+1.871	2447596.57804	0.5604	+1.799
2447593.66938	0.0344	+1.931	2447596.52973	0.4852	+1.871	2447596.57872	0.5615	+1.797
2447593.67009	0.0355	+1.937	2447596.53042	0.4863	+1.876	2447596.58762	0.5753	+1.749
2447593.67077	0.0365	+1.936	2447596.53173	0.4884	+1.871	2447596.58833	0.5764	+1.747
2447593.67226	0.0389	+1.931	2447596.53243	0.4894	+1.878	2447596.58901	0.5775	+1.750
2447593.67296	0.0399	+1.922	2447596.53312	0.4905	+1.878	2447596.58971	0.5786	+1.747
2447593.67365	0.0410	+1.908	2447596.53382	0.4916	+1.873	2447596.59040	0.5796	+1.743
2447593.67435	0.0421	+1.918	2447596.53451	0.4927	+1.877	2447596.59185	0.5819	+1.728
2447593.67504	0.0432	+1.897	2447596.53583	0.4947	+1.873	2447596.59254	0.5830	+1.731
2447593.67737	0.0468	+1.894	2447596.53652	0.4958	+1.872	2447596.59324	0.5841	+1.737
2447593.67807	0.0479	+1.883	2447596.53722	0.4969	+1.875	2447596.59393	0.5851	+1.720
2447596.59463	0.5862	+1.730	2447596.67340	0.7088	+1.501	2447601.43641	0.1203	+1.556
2447596.59839	0.5921	+1.699	2447596.67409	0.7099	+1.497	2447601.43761	0.1222	+1.543
2447596.59908	0.5932	+1.686	2447601.36639	0.0114	+1.969	2447601.43830	0.1233	+1.539
2447596.59978	0.5942	+1.689	2447601.36709	0.0125	+1.960	2447601.43900	0.1243	+1.528
2447596.60047	0.5953	+1.688	2447601.36778	0.0135	+1.968	2447601.43969	0.1254	+1.528
2447596.60116	0.5964	+1.685	2447601.36848	0.0146	+1.962	2447601.44039	0.1265	+1.522
2447596.60268	0.5988	+1.673	2447601.36917	0.0157	+1.957	2447601.44215	0.1293	+1.525
2447596.60338	0.5998	+1.672	2447601.37130	0.0190	+1.962	2447601.44284	0.1303	+1.515
2447596.60407	0.6009	+1.679	2447601.37198	0.0201	+1.955	2447601.44354	0.1314	+1.518
2447596.60476	0.6020	+1.675	2447601.37268	0.0212	+1.956	2447601.44423	0.1325	+1.514
2447596.60546	0.6031	+1.678	2447601.37337	0.0222	+1.952	2447601.44492	0.1336	+1.511
2447596.60667	0.6050	+1.666	2447601.37407	0.0233	+1.949	2447601.44682	0.1365	+1.508
2447596.60737	0.6061	+1.658	2447601.37785	0.0292	+1.938	2447601.44753	0.1376	+1.503
2447596.60806	0.6071	+1.661	2447601.37855	0.0303	+1.944	2447601.44821	0.1387	+1.506
2447596.60876	0.6082	+1.655	2447601.37924	0.0314	+1.938	2447601.44891	0.1398	+1.499
2447596.60945	0.6093	+1.646	2447601.37994	0.0324	+1.931	2447601.44960	0.1408	+1.500
2447596.62018	0.6260	+1.614	2447601.38063	0.0335	+1.934	2447601.45342	0.1468	+1.479
2447596.62089	0.6271	+1.613	2447601.38186	0.0354	+1.938	2447601.45410	0.1478	+1.484
2447596.62157	0.6282	+1.605	2447601.38255	0.0365	+1.934	2447601.45480	0.1489	+1.479
2447596.62226	0.6292	+1.611	2447601.38325	0.0376	+1.921	2447601.45549	0.1500	+1.476
2447596.62296	0.6303	+1.601	2447601.38394	0.0387	+1.928	2447601.45619	0.1511	+1.476
2447596.62435	0.6325	+1.605	2447601.38465	0.0398	+1.917	2447601.45759	0.1533	+1.473
2447596.62504	0.6336	+1.606	2447601.38601	0.0419	+1.913	2447601.45827	0.1543	+1.467
2447596.62574	0.6346	+1.599	2447601.38670	0.0430	+1.906	2447601.45896	0.1554	+1.467
2447596.62643	0.6357	+1.586	2447601.38739	0.0440	+1.898	2447601.45966	0.1565	+1.466
2447596.62713	0.6368	+1.600	2447601.38808	0.0451	+1.890	2447601.46035	0.1576	+1.464
2447596.62817	0.6384	+1.591	2447601.38878	0.0462	+1.890	2447601.46208	0.1603	+1.452
2447596.62885	0.6395	+1.592	2447601.39075	0.0493	+1.875	2447601.46276	0.1613	+1.450
2447596.62954	0.6406	+1.591	2447601.39144	0.0503	+1.868	2447601.46345	0.1624	+1.442
2447596.63024	0.6416	+1.587	2447601.39214	0.0514	+1.858	2447601.46415	0.1635	+1.451
2447596.63093	0.6427	+1.587	2447601.39283	0.0525	+1.862	2447601.46484	0.1646	+1.448
2447596.63627	0.6510	+1.565	2447601.39352	0.0536	+1.850	2447601.47196	0.1756	+1.425
2447596.63696	0.6521	+1.575	2447601.39792	0.0604	+1.809	2447601.47266	0.1767	+1.429
2447596.63766	0.6532	+1.569	2447601.39862	0.0615	+1.800	2447601.47335	0.1778	+1.428
2447596.63835	0.6543	+1.554	2447601.39931	0.0626	+1.789	2447601.47404	0.1789	+1.422
2447596.63905	0.6554	+1.560	2447601.40001	0.0637	+1.796	2447601.47474	0.1800	+1.418
2447596.64042	0.6575	+1.559	2447601.40070	0.0648	+1.781	2447601.47619	0.1822	+1.423
2447596.64112	0.6586	+1.556	2447601.40215	0.0670	+1.771	2447601.47688	0.1833	+1.419
2447596.64182	0.6597	+1.558	2447601.40284	0.0681	+1.766	2447601.47758	0.1844	+1.419
2447596.64251	0.6607	+1.556	2447601.40354	0.0692	+1.759	2447601.47827	0.1855	+1.418
2447596.64320	0.6618	+1.560	2447601.40423	0.0702	+1.755	2447601.47896	0.1865	+1.419
2447596.64473	0.6642	+1.551	2447601.40492	0.0713	+1.744	2447601.48054	0.1890	+1.416
2447596.64829	0.6697	+1.528	2447601.42217	0.0982	+1.619	2447601.48123	0.1901	+1.411
2447596.65154	0.6748	+1.535	2447601.42286	0.0992	+1.617	2447601.48193	0.1912	+1.413
2447596.65223	0.6759	+1.535	2447601.42356	0.1003	+1.615	2447601.48262	0.1922	+1.410
2447596.65294	0.6770	+1.536	2447601.42426	0.1014	+1.611	2447601.48332	0.1933	+1.409
2447596.65362	0.6780	+1.529	2447601.42495	0.1025	+1.607	2447601.48747	0.1998	+1.402

Table 3 – *continued.*

H.J.D.	Phase	(V–C)	H.J.D.	Phase	(V–C)	H.J.D.	Phase	(V–C)
2447596.65431	0.6791	+1.528	2447601.42672	0.1052	+1.604	2447601.48817	0.2009	+1.393
2447596.66336	0.6932	+1.502	2447601.42742	0.1063	+1.601	2447601.48886	0.2019	+1.401
2447596.66406	0.6943	+1.507	2447601.42811	0.1074	+1.598	2447601.48955	0.2030	+1.396
2447596.66475	0.6953	+1.507	2447601.42880	0.1085	+1.586	2447601.49025	0.2041	+1.398
2447596.66545	0.6964	+1.501	2447601.42950	0.1096	+1.591	2447601.49189	0.2066	+1.393
2447596.66614	0.6975	+1.494	2447601.43363	0.1160	+1.562	2447601.49259	0.2077	+1.390
2447596.67132	0.7056	+1.493	2447601.43432	0.1171	+1.557	2447601.49328	0.2088	+1.396
2447596.67201	0.7066	+1.491	2447601.43502	0.1182	+1.561	2447601.49398	0.2099	+1.393
2447596.67270	0.7077	+1.493	2447601.43571	0.1192	+1.561	2447601.49738	0.2152	+1.389
2447601.49807	0.2163	+1.390	2447601.55392	0.3032	+1.426	2447601.62255	0.4100	+1.651
2447601.49877	0.2174	+1.390	2447601.56203	0.3158	+1.436	2447601.62325	0.4111	+1.646
2447601.49946	0.2184	+1.382	2447601.56273	0.3169	+1.442	2447601.62394	0.4121	+1.655
2447601.50016	0.2195	+1.386	2447601.56342	0.3180	+1.445	2447601.63207	0.4248	+1.689
2447601.50653	0.2294	+1.377	2447601.56411	0.3190	+1.451	2447601.63276	0.4259	+1.685
2447601.50723	0.2305	+1.379	2447601.56481	0.3201	+1.448	2447601.63345	0.4269	+1.694
2447601.50792	0.2316	+1.374	2447601.56609	0.3221	+1.452	2447601.63415	0.4280	+1.692
2447601.50862	0.2327	+1.378	2447601.56679	0.3232	+1.460	2447601.63484	0.4291	+1.703
2447601.50931	0.2338	+1.383	2447601.56748	0.3243	+1.460	2447601.63585	0.4307	+1.707
2447601.51060	0.2358	+1.375	2447601.56818	0.3254	+1.459	2447601.63656	0.4318	+1.717
2447601.51129	0.2368	+1.380	2447601.56887	0.3264	+1.460	2447601.63724	0.4328	+1.714
2447601.51198	0.2379	+1.382	2447601.57519	0.3363	+1.482	2447601.63793	0.4339	+1.719
2447601.51268	0.2390	+1.380	2447601.57589	0.3374	+1.489	2447601.63863	0.4350	+1.719
2447601.51339	0.2401	+1.382	2447601.57658	0.3384	+1.487	2447601.63992	0.4370	+1.735
2447601.51700	0.2457	+1.385	2447601.57727	0.3395	+1.489	2447601.64062	0.4381	+1.729
2447601.51769	0.2468	+1.382	2447601.57797	0.3406	+1.494	2447601.64133	0.4392	+1.731
2447601.51839	0.2479	+1.390	2447601.58005	0.3438	+1.500	2447601.64201	0.4402	+1.744
2447601.51908	0.2490	+1.392	2447601.58075	0.3449	+1.507	2447601.64270	0.4413	+1.747
2447601.51977	0.2500	+1.387	2447601.58144	0.3460	+1.504	2447601.65255	0.4566	+1.793
2447601.52126	0.2524	+1.381	2447601.58214	0.3471	+1.505	2447601.65325	0.4577	+1.797
2447601.52195	0.2534	+1.384	2447601.58283	0.3482	+1.508	2447601.65394	0.4588	+1.805
2447601.52264	0.2545	+1.385	2447601.59011	0.3595	+1.521	2447601.65464	0.4599	+1.806
2447601.52334	0.2556	+1.386	2447601.59080	0.3606	+1.525	2447601.65533	0.4610	+1.811
2447601.52403	0.2567	+1.387	2447601.59150	0.3616	+1.526	2447601.65638	0.4626	+1.817
2447601.52585	0.2595	+1.389	2447601.59219	0.3627	+1.525	2447601.65708	0.4637	+1.816
2447601.52654	0.2606	+1.389	2447601.59289	0.3638	+1.529	2447601.65777	0.4648	+1.826
2447601.52724	0.2617	+1.388	2447601.59444	0.3662	+1.533	2447601.65847	0.4659	+1.825
2447601.52795	0.2628	+1.384	2447601.59514	0.3673	+1.537	2447601.65916	0.4669	+1.828
2447601.52863	0.2638	+1.386	2447601.59583	0.3684	+1.542	2447601.66040	0.4689	+1.826
2447601.53129	0.2680	+1.392	2447601.59653	0.3695	+1.542	2447601.66109	0.4699	+1.841
2447601.53198	0.2690	+1.390	2447601.59722	0.3705	+1.543	2447601.66179	0.4710	+1.839
2447601.53269	0.2701	+1.388	2447601.60222	0.3783	+1.561	2447601.66248	0.4721	+1.845
2447601.53337	0.2712	+1.390	2447601.60291	0.3794	+1.567	2447601.66318	0.4732	+1.843
2447601.53407	0.2723	+1.394	2447601.60361	0.3805	+1.566	2447601.67020	0.4841	+1.865
2447601.53599	0.2753	+1.395	2447601.60430	0.3816	+1.567	2447601.67090	0.4852	+1.873
2447601.53668	0.2763	+1.396	2447601.60499	0.3826	+1.577	2447601.67159	0.4863	+1.874
2447601.53738	0.2774	+1.402	2447601.60841	0.3880	+1.586	2447601.67229	0.4874	+1.872
2447601.53807	0.2785	+1.402	2447601.60911	0.3891	+1.586	2447601.67298	0.4884	+1.873
2447601.53877	0.2796	+1.400	2447601.60980	0.3901	+1.581	2447601.67426	0.4904	+1.863
2447601.54273	0.2858	+1.404	2447601.61049	0.3912	+1.592	2447601.67496	0.4915	+1.872
2447601.54342	0.2868	+1.409	2447601.61119	0.3923	+1.592	2447601.67565	0.4926	+1.873
2447601.54411	0.2879	+1.412	2447601.61315	0.3953	+1.600	2447601.67635	0.4937	+1.870
2447601.54481	0.2890	+1.407	2447601.61385	0.3964	+1.601	2447601.67704	0.4948	+1.870
2447601.54550	0.2901	+1.413	2447601.61454	0.3975	+1.611	2447601.67832	0.4967	+1.866
2447601.54687	0.2922	+1.415	2447601.61524	0.3986	+1.611	2447601.67901	0.4978	+1.875
2447601.54756	0.2933	+1.417	2447601.61593	0.3997	+1.614	2447601.67970	0.4989	+1.873
2447601.54826	0.2944	+1.418	2447601.61727	0.4017	+1.616	2447601.68040	0.5000	+1.873
2447601.54895	0.2954	+1.413	2447601.61797	0.4028	+1.622	2447601.68109	0.5011	+1.870
2447601.54965	0.2965	+1.422	2447601.61866	0.4039	+1.623	2447601.68209	0.5026	+1.871
2447601.55114	0.2988	+1.424	2447601.61936	0.4050	+1.627	2447601.68279	0.5037	+1.872
2447601.55183	0.2999	+1.427	2447601.62005	0.4061	+1.627	2447601.68348	0.5048	+1.875
2447601.55253	0.3010	+1.424	2447601.62116	0.4078	+1.639	2447601.68417	0.5058	+1.874
2447601.55322	0.3021	+1.432	2447601.62186	0.4089	+1.645	2447601.68487	0.5069	+1.878

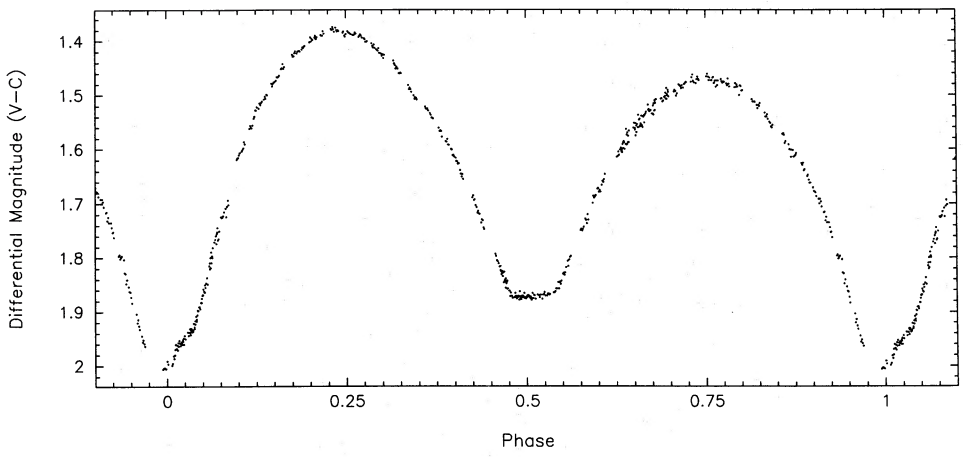

Figure 3. 1989 TPT V observations of AG Vir in the sense variable minus comparison between AG Vir and BD + 13° 2485.

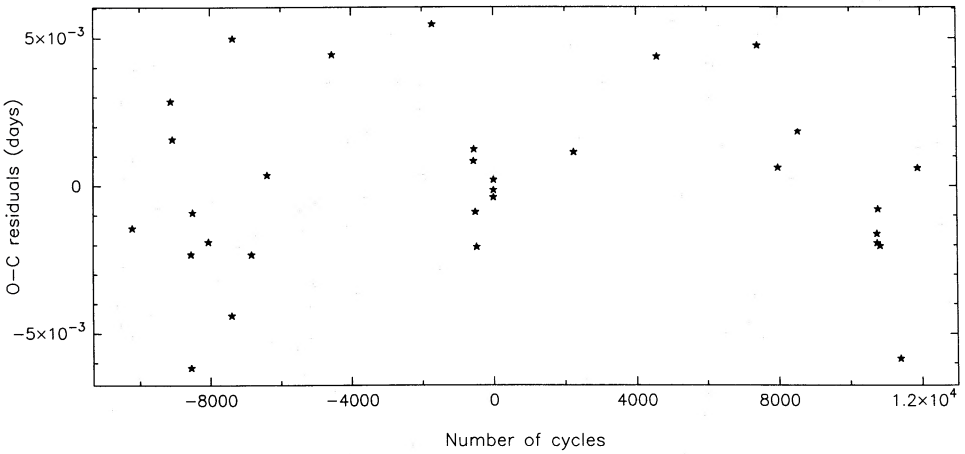

Figure 4. Observed minus calculated times of minima in fractions of a day based on the period determined from 31 photoelectric times of primary minima since 1944. Cycle numbers are derived from the ephemeris computed by Binnendijk (1969).

gested that secondary minima may be more appropriate for use in period determinations as the phase interval 0ᵖ41–0ᵖ59 is relatively free from distortion. However, determinations of secondary minima are still few in number and the photometric data presented here do not support this suggestion. Most observers have avoided the distorted section at the bottom of primary minimum for their time of minimum and period determinations and this practice has been continued for this study.

One primary and one secondary minimum have been determined from the observations presented here using the method of Kwee & van Woerden (1956), omitting the distorted sections at the bottom of both minima. A least-squares analysis of 31 times of primary minimum since 1944 was made to calculate the period of AG Vir on the assumption that the period has been constant during that interval. The $O-C$ residuals from the period determination are plotted against the cycle numbers derived from Binnendijk's ephemeris in Fig. 4. The ephemeris that follows is composed of the primary minimum derived from the TPT data and the period determined in the least-squares analysis and has been used to phase the spectroscopic and photometric data presented in this study.

Primary minimum (HJD) = 2447593.64729
(± 0.00011) + 0.64265059 (± 0.00000007).E.

Using this ephemeris, the residuals of 72 visual, photographic and photoelectric times of minima summarized in Table 4 are plotted in Fig. 5. The photoelectric data show a scatter of approximately 0.005 d, whereas that for the visual data is some 10 times higher. Clearly, visual observations of the distorted minima of AG Vir are of limited value and photoelectric determinations offer the only reliable way to evaluate the times of minima for this system.

5 PHOTOMETRIC ANALYSIS

5.1 Spectral type and colour indices

In his study of AG Vir, Wood (1946) estimated the spectral types of the components of the system to be A2 + A9. Hill & Barnes (1972) were unable to detect the secondary component on their spectra and classified the brighter component to be between A7 and A9. This classification has subsequently been confirmed by Hill *et al.* (1975).

Table 4. Times of minima for AG Vir.

H.J.D.	Cycle	Method	Reference
2424585.494	−23903.0	PG	Prager & Dugan (Wood, 1946)
2425002.575	−23254.0	PG	Prager & Dugan (Wood, 1946)
2425004.520	−23251.0	PG	Prager, 1929
2425740.325	−22106.0	VIS	Kukarkin, 1929.
2426117.562	−21519.0	PG	Dugan (Wood, 1946)
2426119.496	−21516.0	PG	Dugan (Wood, 1946)
2426124.660	−21508.0	PG	Dugan (Wood, 1946)
2426418.991	−21050.0	PG	Bodokia, 1937
2426444.701	−21010.0	PG	Dugan (Wood, 1946)
2427157.381	−19901.0	VIS	Kreiner, 1976
2427547.499	−19294.0	VIS	Lause, 1937
2427888.714	−18763.0	PG	Dugan (Wood, 1946)
2427891.610	−18758.5	PG	Dugan (Wood, 1946)
2428297.440	−18127.0	VIS	Lause, 1937
2428612.341	−17637.0	VIS	Lause, 1937
2429329.851	−16520.5	PE	Wood, 1946
2429334.993	−16512.5	PE	Wood, 1946
2429335.956	−16511.0	PE	Wood, 1946
2429337.884	−16508.0	PE	Wood, 1946
2429338.851	−16506.5	PE	Wood, 1946
2429339.811	−16505.0	PE	Wood, 1946
2429346.879	−16494.0	PE	Wood, 1946
2429359.734	−16474.0	PE	Wood, 1946
2429363.910	−16467.5	PE	Wood, 1946
2429368.732	−16460.0	PE	Wood, 1946
2431265.173	−13509.0	VIS	Zessewitch, 1944
2433387.854	−10206.0	PE	Nason & Moore, 1951
2434086.41948	−9119.0	PE	Kwee, 1958
2434120.47868	−9066.0	PE	Kwee, 1958
2434455.2919	−8545.0	PE	Szczepanowska, 1958
2434458.5090	−8540.0	PE	Szczepanowska, 1958
2434487.42968	−8495.0	PE	Kwee, 1958
2434776.62146	−8045.0	PE	Kwee, 1958
2435197.5551	−7390.0	PE	Szczepanowska, 1958
2435198.5286	−7388.5	PE	Szczepanowska, 1958
2435219.4146	−7356.0	PE	Szczepanowska, 1958
2435561.2974	−6824.0	PE	Szczepanowska, 1958
2435562.2619	−6822.5	PE	Szczepanowska, 1958
2435848.5649	−6377.0	PE	Szczepanowska, 1958
2437028.47545	−4541.0	PE	Purgathofer & Widorn, 1964
2438846.5350	−1712.0	PE	Blanco & Catalano, 1970
2439587.5065	−559.0	PE	Blanco & Catalano, 1970
2439596.5040	−545.0	PE	Blanco & Catalano, 1970
2439618.3520	−511.0	PE	Blanco & Catalano, 1970
2439643.4142	−472.0	PE	Blanco & Catalano, 1970
2439943.8593	−4.5	PE	Binnendijk, 1969
2439944.8190	−3.0	PE	Binnendijk, 1969
2439946.7472	0.0	PE	Binnendijk, 1969
2439948.6755	3.0	PE	Binnendijk, 1969
2441391.4270	2248.0	PE	Kizilirmak & Pohl, 1974
2442451.4800	3897.5	PE	Pohl & Kizilirmak, 1976
2442892.6620	4584.0	PE	Mallama *et al.*, 1977
2444709.4356	7411.0	PE	Pohl *et al.*, 1982
2445074.457	7979.0	PE	Locher, 1982
2445432.4146	8536.0	PE	Niarchos, 1985
2445433.3851	8537.5	PE	Niarchos, 1985
2445741.2071	9016.5	PE	Kałużny, 1986
2446113.630	9648.5	VIS	Isles, 1989
2446180.409	9700.0	VIS	Locher, 1985
2446855.8822	10751.0	PE	Michaels, 1988
2446859.7378	10757.0	PE	Michaels, 1988
2446860.7106	10758.5	PE	Michaels, 1988
2446875.8052	10782.0	PE	Michaels, 1988
2446892.505	10808.0	VIS	Locher, 1987
2446903.42	10825.0	VIS	Locher, 1987
2446911.7924	10838.0	PE	Michaels, 1988
2447261.3930	11382.0	VIS	Hübscher & Lichtenknecker, 1988
2447262.3659	11383.5	PE	Keskin & Pohl, 1989
2447270.3876	11396.0	PE	Locher, 1988
2447270.404	11396.0	VIS	Locher, 1988
2447593.6473	11899.0	PE	TPT — this paper
2447596.5443	11903.5	PE	TPT — this paper

Eggen (1967) published $(B-V)$ colour indices for AG Vir of 0.31 and 0.29 mag for phases close to primary and secondary minimum, respectively, and determined a colour excess $E(B-V)$ of $+0.03$ mag for the system. The period–colour relation plotted by Eggen shows that AG Vir lies in an area between regions occupied by detached and contact systems at an age of about 5×10^8 yr. More recently, Hilditch & Hill (1975) have published several Strömgren colour indices at secondary minimum indicating a mean $(b-y)$ of 0.161 mag. Similarly, Rucinski & Kałużny (1981) published a mean $(b-y)$ for the system of 0.156 mag. Using the spectrum–colour relation given by Rucinski & Kałużny, the dereddened $(b-y)$ colour index of Hilditch & Hill would indicate a spectral type of A9 whereas that of Rucinski & Kałużny indicates A8.

Assuming $E(b-y)=0.74\ E(B-V)$, and that the $(B-V)$ colour excess given by Eggen is correct, then $(b-y)_0=0.14$ mag at secondary minimum. If the contribution of the secondary component to the total light of the system is negligible at secondary minimum then a temperature for the primary component of 7400 K can be inferred using the $(b-y)_0$–temperature tabulation given by Popper (1980). This compares favourably with the spectral classification of between A7 and A9. From the $(B-V)_0$–effective temperature

calibration of Böhm-Vitense (1981), the $(B-V)$ colour index given by Eggen suggests a temperature for the primary component of 7500 ± 200 K. According to Böhm-Vitense, this estimate places the primary component at the limiting temperature for which models incorporating radiative equilibrium are required for single stars. For this study, a temperature estimate for the primary component of 7400 ± 200 K has been adopted.

5.2 Light-curve analysis

Each half of the TPT light curve for AG Vir was analysed separately using the light-curve synthesis program LIGHT2 (G. Hill, private communication), an expanded version of LIGHT (Hill 1979). Contact solutions were initiated with an inclination i of 80°, a 'fill-out' factor f as defined by Rucinski (1973) of 1.0 (denoting marginal contact), and the mass ratio q fixed at that derived spectroscopically. Similarly, the detached solutions were started with the primary and secondary mean radii, $\bar{r}_1$ and $\bar{r}_2$, respectively, set to 0.45 and 0.25. Bolometric albedos α_1 and α_2 for the primary and secondary components, respectively, were both fixed at 0.5, and solutions were attempted with the gravity-darkening exponents β_1 and β_2 for both the primary and secondary components fixed at their convective values of 0.08 and also their radiative values of 0.25. The primary component temperature T_1 was fixed at 7400 K and solutions were sought for the inclination, fill-out factor or mean radii and secondary component temperature T_2.

The preliminary analysis suggested three methods of solution for each half of the light curve. Two contact-mode solutions were made, one using $\beta_{1,2} = 0.25$ and the other using $\beta_{1,2} = 0.08$. A detached-mode solution using $\beta_1 = 0.25$ and $\beta_2 = 0.08$ was also attempted. The results for the solutions of the first half of the light curve are given in Table 5 and those for the second half are given in Table 6. The convective-contact, radiative-contact and detached-mode solutions for each half of the light curve are shown in Figs 6, 7 and 8, respectively. The solutions have been reflected around 0$^{\rm p}$.5 and plotted against the complete set of data. The residuals for each half of the light curve from their respective solutions have also been plotted in Figs 6, 7 and 8.

The solutions obtained for the first half of the light curve indicate a system whose inclination is very close to 90°. The detached-mode solution shown in Fig. 8 is clearly inadequate as very little of the curve is fitted properly. The contact-mode solutions do appear to be a reasonable fit to the majority of the data with the exception of 0$^{\rm p}$.4 to 0$^{\rm p}$.5 where the fit is in error by up to 0.03 mag. Both of the contact-mode solutions indicate deep-contact configurations with a secondary component whose temperature is between 400 and 700 K cooler than that of the primary component. Although the convective contact-mode solution appears to be the best fit to the first half of the light curve, in general, contact systems with this degree of contact ($f \simeq 0.5$–0.6) normally exhibit smaller temperature differences between the two components ($\leqslant 100$ K) and consequently these solutions for AG Vir should be treated with some caution.

The two contact-mode solutions to the second half of the light curve are of similar quality. They are both 0.02 mag too deep at secondary minimum and are up to 0.05 mag too deep at primary minimum. These solutions indicate a marginal-contact system at an inclination close to 90° with a temperature difference between the two components of between 500 and 800 K. The detached-mode solution is the most satisfactory overall fit to the data in the second half of the light curve, fitting the depths of the minima better than the contact-mode solutions. This solution indicates that the system is very close to or just in contact with an inclination of 81° and a secondary component temperature 1100 K cooler than that of the primary.

It would appear that each half of the light curve can be fitted moderately well by quite different system configurations. The first half of the curve suggests a deep-contact system whereas the second half indicates a marginal-contact system. If the deep-contact configuration is adopted then the fainter second quadrature could be explained by an area of reduced luminosity on one (or both) of the components. Similarly, if the marginal-contact configuration is to be believed then the brighter first quadrature may be caused by an area of enhanced luminosity on one (or both) of the components. The presence of hot or cool spots on one or both of the components is discussed in Section 5.3. For the spot modelling in the following section, the deep-contact solution with $\beta_{1,2} = 0.08$ has been adopted as the best fit to the first half of the light curve, whereas the detached-mode solution has been adopted for the second half of the light curve.

5.3 Spot modelling

LIGHT2 was used to examine the effect on the observed light curve of spots of various types and at various locations on both components of the system. In each case the spot was assumed to be circular and to have a latitude of 0°. The spot longitude is defined as the angle between the sub-stellar point and the spot measured anti-clockwise from the sub-stellar point as seen from the north pole of the given star. The spot temperature is expressed as an excess over the photospheric temperature of the component on which the spot is located. Any attempt to use a single-colour light curve to solve for a *unique* radius and temperature of a spot will fail unless the spot radius can be constrained by geometrical considerations or the spot temperature can be estimated from another source. Unlike BX And (Bell *et al.* 1990), the spot radius for AG Vir cannot be constrained by geometrical considerations, and consequently test solutions to determine spot radius and excess temperature using LIGHT2 failed. In an attempt to keep the spot modelling as simple as possible, the effects of a single spot on either of the components have been examined in preference to those caused by multiple spots on both components.

Four possible spot configurations can be put forward to explain the disparity in the quadrature brightnesses. For the deep-contact configuration, two cool-spot geometries could be adopted to mimic the observations – a cool spot at a longitude of approximately 270° on the secondary component or a cool spot on the primary component at a longitude of approximately 90°. Similarly, for the marginal-contact configuration, two hotspot geometries can be used – a hotspot on the primary at a longitude of approximately 270° or a hotspot on the secondary at a longitude of approximately 90°. LIGHT2 was used to generate light curves using both the

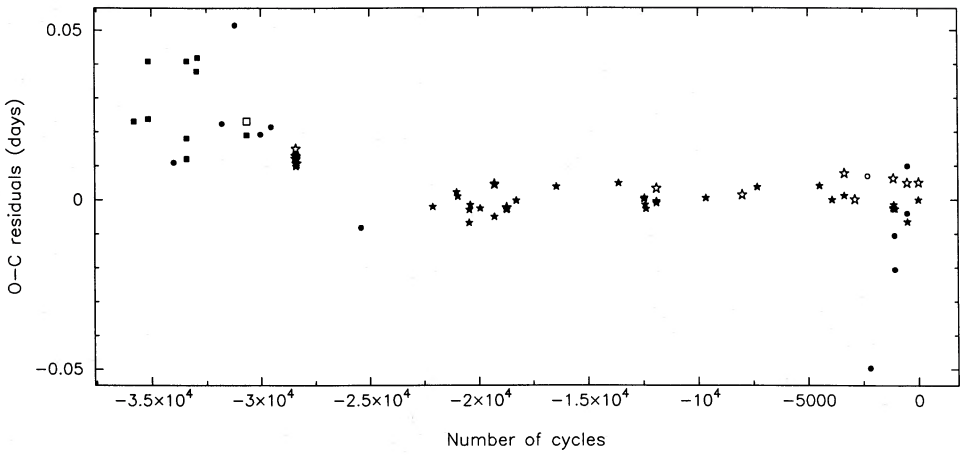

Figure 5. Observed minus calculated times of minima in fractions of a day based on the ephemeris computed in Section 4 using published data and those minima obtained for this study. Filled symbols represent primary minima and open symbols represent secondary minima. Squares indicate data acquired photographically, circles those estimated visually and stars for those minima measured photoelectrically.

Table 5. LIGHT2 solutions for data from 0P0 to 0P5.

Solution	Contact mode	Contact mode	Detached mode
parameter	$\beta_{1,2} = 0.08$	$\beta_{1,2} = 0.25$	$\beta_1 = 0.25$, $\beta_2 = 0.08$
T_2 (K)	7000 ± 11	6683 ± 13	6398 ± 28
i (°)	89.26 ± 0.16	88.96 ± 0.16	90.00 (†)
f	0.523 ± 0.013	0.712 ± 0.013	see $\overline{r_1}$ & $\overline{r_2}$
$\overline{r_1}$	0.514 ± 0.001	0.503 ± 0.001	0.484 ± 0.003
$\overline{r_2}$	0.315 ± 0.001	0.303 ± 0.001	0.282 ± 0.002
$\alpha_{1,2}$	0.50 (fixed)	0.50 (fixed)	0.50 (fixed)
χ^2	1.783×10^{-4}	1.577×10^{-4}	7.416×10^{-4}
$\overline{O-C}$ & s.d.	0.0000 ± 0.0122	-0.0001 ± 0.0116	-0.0019 ± 0.0256

†This quantity was fixed during the solution process.

Table 6. LIGHT2 solutions for data from 0P5 to 1P0.

Solution	Contact mode	Contact mode	Detached mode
parameter	$\beta_{1,2} = 0.08$	$\beta_{1,2} = 0.25$	$\beta_1 = 0.25$, $\beta_2 = 0.08$
T_2 (K)	6879 ± 19	6576 ± 21	6293 ± 21
i (°)	87.35 ± 0.19	89.02 ± 0.26	81.04 ± 0.51
f	0.924 ± 0.022	1.000 (†)	see $\overline{r_1}$ & $\overline{r_2}$
$\overline{r_1}$	0.491 ± 0.002	0.484 ± 0.001	0.484 ± 0.002
$\overline{r_2}$	0.289 ± 0.001	0.283 ± 0.001	0.280 ± 0.002
$\alpha_{1,2}$	0.50 (fixed)	0.50 (fixed)	0.50 (fixed)
χ^2	3.704×10^{-4}	3.426×10^{-4}	2.088×10^{-4}
$\overline{O-C}$ & s.d.	0.0005 ± 0.0179	$+0.0006 \pm 0.0171$	-0.0003 ± 0.0137

†This quantity was fixed during the solution process.

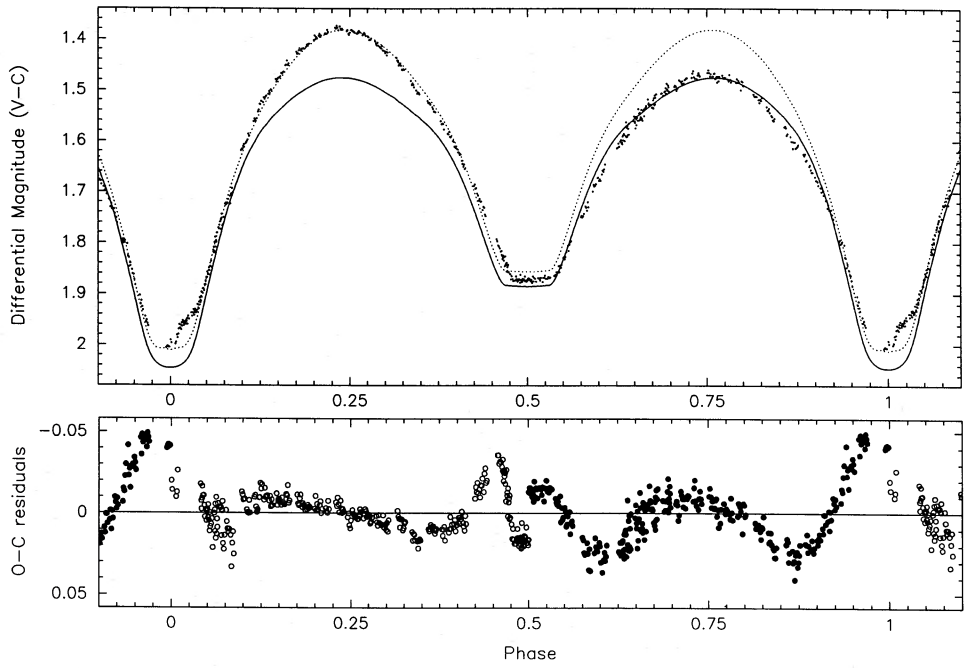

Figure 6. The upper plot shows the TPT V observations of AG Vir and two convective contact solutions for each half of the light curve. The dotted line is a solution to the light curve from 0P0 to 0P5 and the solid line is a solution to the light curve from 0P5 to 1P0. The lower plot shows the residuals of the data from each half of the light curve and its respective solution. The open symbols represent the first half of the light curve and the filled symbols the second half of the light curve.

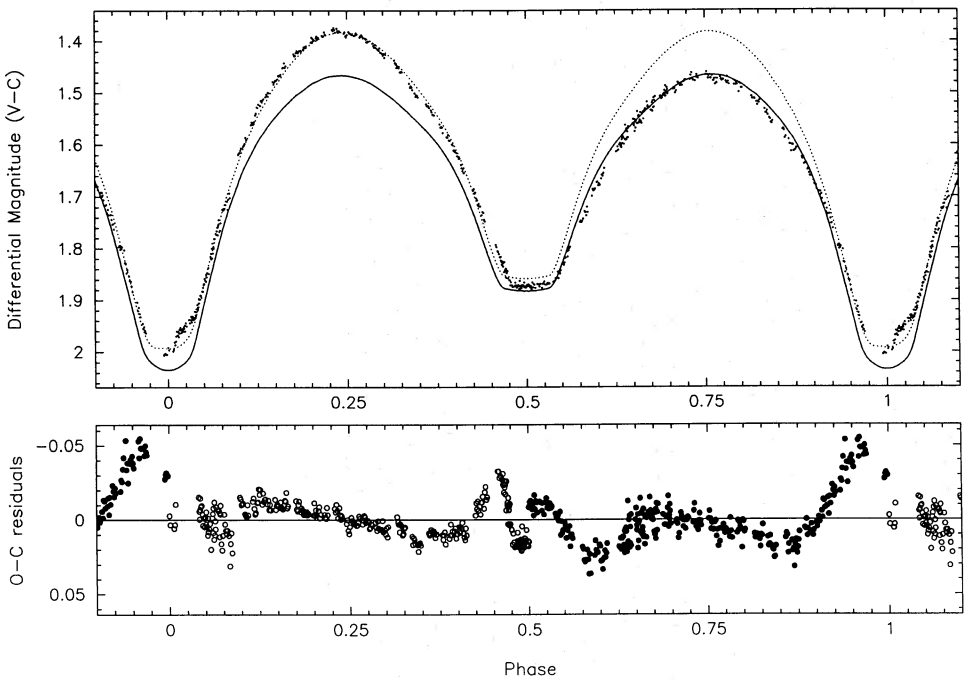

Figure 7. The upper plot shows the TPT V observations of AG Vir and two radiative contact solutions for each half of the light curve. The lines and symbols have the same meaning as Fig. 6.

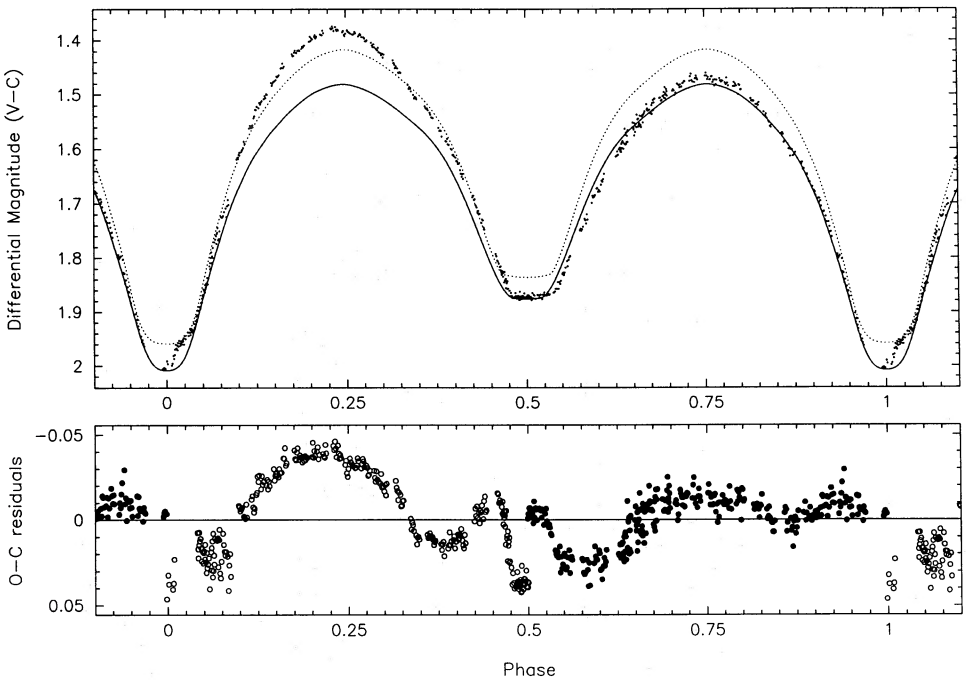

Figure 8. The upper plot shows the TPT V observations of AG Vir and two detached solutions for each half of the light curve. The lines and symbols have the same meaning as Fig. 6.

deep-contact and marginal-contact configurations with spot excess temperatures in the range −3000 to +3000 K in steps of 500 K and spot radii in the range 10° to 40° in steps of 10°. This technique cannot produce a unique spot radius and excess temperature; however, a satisfactory match does indicate that the presence of spots is a viable explanation for the appearance of the light curve. The four best matches are given in Table 7 and displayed in Figs 9 and 10.

The problem of uniqueness can be addressed by using Doppler-imaging techniques to identify the component of the system on which the spot resides and *simultaneous* infrared and visual photometry can be employed to estimate the

spot temperature. The predicted (V–K) colours for the four spot models are given in Figs 9 and 10. These colours have been synthesized using LIGHT2 relative to the colour of the system at secondary minimum. At this point in the orbital cycle only the primary component is visible and the absolute (V–K) colour has been fixed using the tabulation of intrinsic colours given by Koornneef (1983). If (V–K) colours accurate to ≈ 0.02 mag were available, they could be used to discriminate between the deep-contact and marginal-contact models. It should be noted that these colours are of no assistance in determining upon which component the spot resides. The closest colour index to (V–K) currently known to the authors is unpublished BVR photometry of AG Vir obtained at the University of Victoria, British Columbia (R. Robb, private communication), which indicates that the (V–R) and (B–R) colours are bluest around 0^{p}2 and shows a gradual reddening towards primary minimum. Although the scatter is around 0.04 mag, this photometry does favour the suggestion that a spot is present on one of the components. Only Doppler imaging via high-resolution spectroscopy can provide the necessary spatial information on the spot location and this technique, in conjunction with simultaneous optical and infrared photometry, provides the best opportunity of obtaining a unique solution to the AG Vir light curve.

In order to test the validity of the original analysis, the generated light curves were solved in the same manner as the observed light curve of AG Vir. A solution for the fill-out factor, secondary component temperature and inclination was made for each half of the light curve making no allowance for the presence of the spot. Solutions to the second half of the light curves generated using a deep-contact configuration and a cool spot on either component indicated marginal-contact solutions, however, the secondary temperature did show a discrepancy of 200 K. Similarly, the first half of the light curves generated using a marginal-contact configuration and a hotspot on either component yielded deep-contact solutions with $0.5 < f < 0.6$ and a secondary component temperature of 7100 K. In all cases, the inclination showed little deviation from the original values.

The asymmetry in the primary minimum may also be explained in terms of a spot. This feature can be seen in several of the published light curves and normally appears between 0^{p}00 and 0^{p}04. This suggests that the spot is a region of enhanced luminosity on the primary component which is eclipsed at 0^{p}04 by the secondary component. If this is the case, it should become visible once more at approximately 0^{p}6 and be viewed 'face-on' at approximately 0^{p}8. If the deep-contact model is adopted, the effect of this hotspot is to reduce the contribution of the proposed cool spot at or just after second quadrature. If the marginal-contact configuration is adopted, the hotspot may affect the underlying geometry of the solution.

Table 7. Spot parameters for generated models.

a) Deep contact configuration

Component	Spot longitude	Spot radius	Spot excess temperature
Primary	90°	20°	−2000 K
Secondary	270°	40°	−1500 K

b) Marginal contact configuration

Component	Spot longitude	Spot radius	Spot excess temperature
Primary	270°	20°	+3000 K
Secondary	90°	20°	+1000 K

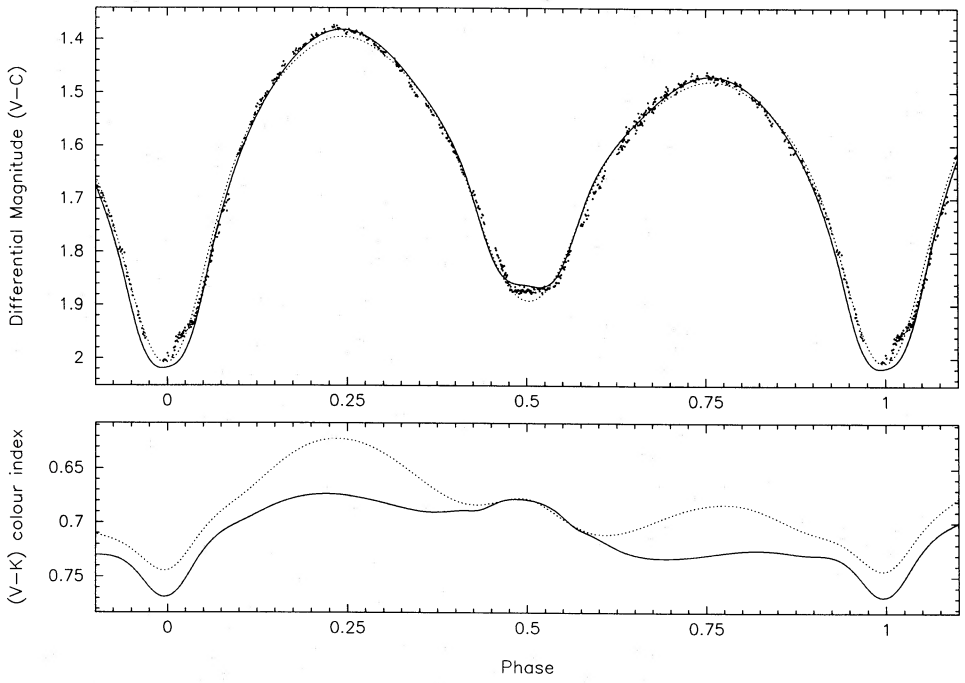

Figure 9. The upper plot shows TPT V observations of AG Vir and models for spots located on the primary component. The solid line is the deep-contact/cool-spot model and the dotted line is the marginal-contact/hotspot model. The lower plot shows the predicted (V–K) colours for the above models. The solid line represents the deep-contact/cool-spot model and the dotted line the marginal-contact/hotspot model.

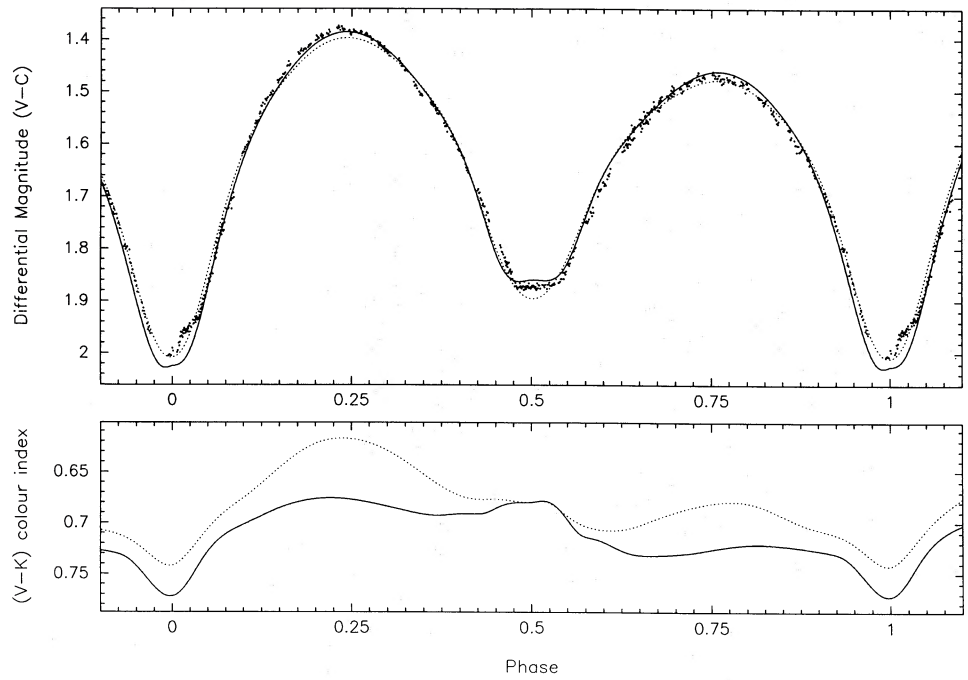

Figure 10. The upper plot shows TPT V observations of AG Vir and models for spots located on the secondary component. The lower plot shows the predicted (V–K) colours for the above models. The lines have the same meaning as Fig. 9.

Table 8. Astrophysical data for AG Vir.

(a) Deep-contact configuration

Absolute dimensions	Primary	Secondary
$M(M_\odot)$	1.61 ± 0.03	0.51 ± 0.01
$R(R_\odot)$	2.07 ± 0.02	1.27 ± 0.01
$log\, g$ (cgs)	4.01 ± 0.01	3.94 ± 0.01
T_{eff} (K)	7400 ± 200	7000 ± 200
$log\, L/L_\odot$	1.06 ± 0.05	0.54 ± 0.06
M_{bol}	$2^m.10 \pm 0^m.12$	$3^m.41 \pm 0^m.13$
B.C.	$-0^m.01$	$-0^m.01$
M_V	$2^m.11 \pm 0^m.12$	$3^m.42 \pm 0^m.13$
$E_{(B-V)}$	$+0^m.03$	
Distance (pc)	193 ± 17	

(b) Marginal contact configuration

Absolute dimensions	Primary	Secondary
$M(M_\odot)$	1.67 ± 0.03	0.53 ± 0.01
$R(R_\odot)$	1.97 ± 0.02	1.14 ± 0.01
$log\, g$ (cgs)	4.07 ± 0.01	4.05 ± 0.01
T_{eff} (K)	7400 ± 200	6300 ± 200
$log\, L/L_\odot$	1.02 ± 0.05	0.27 ± 0.06
M_{bol}	$2^m.21 \pm 0^m.12$	$4^m.10 \pm 0^m.14$
B.C.	$-0^m.01$	$-0^m.06$
M_V	$2^m.22 \pm 0^m.12$	$4^m.16 \pm 0^m.14$
$E_{(B-V)}$	$+0^m.03$	
Distance (pc)	174 ± 14	

6 DISCUSSION

The two adopted photometric solutions are that of the convective contact-mode solution for the first half of the TPT light curve in Table 5 and the detached-mode solution for the second half of the TPT data given in Table 6. Astrophysical data for these two configurations of AG Vir are given in Table 8. An error of 200 K has been adopted in the secondary component temperature as the errors quoted in Tables 5 and 6 take no account of the uncertainty in the primary component temperature. The bolometric corrections employed in the calculation of absolute magnitudes and the distance have been taken from the compilation of Popper (1980).

A comparison of the masses, radii, temperatures and luminosities of the components of AG Vir with those of other marginal-contact and contact binaries compiled by Hilditch, King & McFarlane (1988), shows that the primary component defined by both solutions lies close to the TAMS relationship of Vandenberg (1985) and has properties similar to the A-type contact binaries and the B-type marginal-contact systems. Similarly, the secondary component defined by both solutions is approximately 2.5 times larger than expected for its ZAMS mass and occupies the same region in the M–R and M–L diagrams as other A- and B-type secondary components. The deep-contact secondary component lies just to the left of the ZAMS line in the HR diagram as do some of the hotter secondaries of the A-type systems. The marginal-contact secondary component lies just to the right of the ZAMS relation which may indicate that the luminosity transfer suggested for the W-type systems is not complete but has progressed further than in systems such as RT Scl, RS Ind and BX And (Bell *et al.* 1990) where the secondary component lies to the right of the ZAMS line in the HR diagram. In common with BX And, AG Vir has greater specific orbital

angular momentum than W-type contact binaries of the same mass ratio and has similar specific angular momentum as other B-type systems.

The apparent configuration of AG Vir seems to depend significantly on the type of spot model adopted. It is difficult to see why a hotspot should exist on either component perpendicular to the line of centres of the stars. There is no conclusive evidence for ongoing period variations which would support the presence of mass transfer between the components and there is no room in the system for an accretion stream. Cool spots appear to be the more likely option, since the system is composed of two rapidly rotating stars with convective envelopes, and current knowledge of astrophysics would then expect substantial magnetic activity of which cool starspots are the most readily observed manifestation (e.g. Rucinski 1986). If this is correct, then AG Vir is indeed an A-type system showing considerable spot activity on one of its components. Simultaneous infrared and visual photometry of this system in conjunction with Doppler imaging may hold the key to understanding the nature of this system.

ACKNOWLEDGMENTS

PPR would like to express his gratitude for the assistance extended to him by the staff of the Observatorio del Roque de los Muchachos. We acknowledge PATT for the allocation of observing time, and the SERC for financial support in the form of a research studentship for PPR and a post-doctoral research assistantship for SAB. We are also indebted to Graham Hill for continual improvements to LIGHT2.

REFERENCES

Bell, S. A. & Hilditch, R. W., 1984. *Mon. Not. R. astr. Soc.,* **211,** 229.
Bell, S. A., Rainger, P. P., Hill, G. & Hilditch, R. W., 1990. *Mon. Not. R. astr. Soc.,* **244,** 328.
Binnendijk, L., 1969. *Astr. J.,* **74,** 1024.
Blanco, C. & Catalano, F., 1970. *Mem. Soc. astr. Ital.,* **41,** 343.
Böhm-Vitense, E., 1981. *Ann. Rev. Astr. Astrophys.,* **19,** 295.
Bodokia, V. M., 1937. *Abastumani Bull.,* No. 1, 25.
Dugan, R. S., 1933. *Astr. Nachr.,* **247,** 357.
Eaton, J. A., 1983. *Astrophys. J.,* **268,** 800.
Eggen, O. J., 1967. *Mem. R. astr. Soc.,* **70,** 111.
Fliegel, H. F., 1963. *Dissertation,* University of Pennsylvania.
Gaposchkin, S., 1953. *Harvard Ann.,* **113,** 69.
Guthnick, P. & Prager, R., 1929. *Beob. Zir.,* No. 11, 32.
Hilditch, R. W., 1981. *Mon. Not. R. astr. Soc.,* **196,** 305.
Hilditch, R. W. & Hill, G., 1975. *Mem. R. astr. Soc.,* **79,** 101.
Hilditch, R. W., King, D. J. & McFarlane, T. M., 1988. *Mon. Not. R. astr. Soc.,* **231,** 341.
Hill, G., 1979. *Publs Dom. astrophys. Obs.,* **15,** 297.
Hill, G., 1982. *Publs Dom. astrophys. Obs.,* **16,** 59.
Hill, G. & Barnes, J. V., 1972. *Publs astr. Soc. Pacif.,* **84,** 382.
Hill, G., Hilditch, R. W., Younger, F. & Fisher, W. A., 1975. *Mem. R. astr. Soc.,* **79,** 131.
Hill, G., Fisher, W. A. & Poeckert, R., 1982. *Publs Dom. astrophys. Obs.,* **16,** 43.
Hübscher, J. & Lichtenknecker, D., 1988. *BAV Mitt.,* No. 50.
Isles, J. E., 1989. *BAA Var. Star Section Circ.,* No. 69.
Kałużny, J., 1986. *Acta Astr.,* **36,** 121.
Keskin, V. & Pohl, E., 1989. *Inf. Bull. Var. Stars,* No. 3355.
Kizilirmak, A. & Pohl, E., 1974. *Inf. Bull. Var. Stars,* No. 937.
Koornneef, J., 1983. *Astr. Astrophys.,* **128,** 84.
Kreiner, J. M., 1976. *Acta Astr.,* **26,** 341.
Kwee, K. K., 1958. *Bull. astr. Insts Neth.,* **14,** 131.
Kwee, K. K. & van Woerden, H., 1956. *Bull. astr. Insts Neth.,* **12,** 327.
Kukarkin, B. W., 1929. *Nishni Novgorod Veränd. Sterne,* **1,** No. 12.
Lause, F., 1937. *Astr. Nachr.,* **264,** 107.
Locher, K., 1982. *BBSAG Bull.,* No. 60.
Locher, K., 1985. *BBSAG Bull.,* No. 77.
Locher, K., 1987. *BBSAG Bull.,* No. 83.
Locher, K., 1988. *BBSAG Bull.,* No. 88.
Mallama, A. D., Skillman, D. R., Pinto, P. A. & Krobousek, B. A., 1977. *Inf. Bull. Var. Stars,* No. 1249.
Michaels, E. J., 1988. *Inf. Bull. Var. Stars,* No. 3202.
Nason, M. E. & Moore, R. C., 1951. *Astr. J.,* **56,** 183.
Niarchos, P. G., 1985. *Astr. Astrophys. Suppl.,* **61,** 313.
Pohl, E. & Kizilirmak, A., 1976. *Inf. Bull. Var. Stars,* No. 1163.
Pohl, E., Evren, S., Tümer, O. & Sezer, C., 1982. *Inf. Bull. Var. Stars,* No. 2189.
Popper, D. M., 1980. *Ann. Rev. Astr. Astrophys.,* **18,** 115.
Prager, R., 1929. *Kl. Veröff., Berlin–Babelsberg,* No. 6, 35.
Purgathofer, A. & Widorn, T., 1964. *Mitt. Wein,* **12,** 31.
Rucinski, S. M., 1973. *Acta Astr.,* **24,** 119.
Rucinski, S. M., 1986. In: *Instrumentation and research programmes for small telescopes, IAU Symp. No. 118,* p. 159, eds Hearnshaw, J. B. & Cottrell, P. L., Reidel, Dordrecht, Holland.
Rucinski, S. M. & Kałużny, J., 1981. *Acta Astr.,* **31,** 409.
Sanford, R. F., 1934. *Astrophys. J.,* **79,** 89.
Skillen, W. J., 1985. *PhD thesis,* University of St. Andrews.
Szczepanowska, A., 1958. *Acta Astr.,* **8,** 36.
Vandenberg, D. A., 1985. *Astrophys. J. Suppl.,* **58,** 711.
Wood, F. B., 1946. *Contr. Princeton Univ. Obs.,* No. 21, 4.
Zessewitch, W., 1944. *Kasan Astron. Circ.,* No. 35, 9.